Environmental Research 261 (2024) 119764

Contents lists available at ScienceDirect

Environmental Research

journal homepage: www.elsevier.com/locate/envres

Integrated multi-omics analyses reveal microbial community resilience to fluctuating low oxygen in the East China sea

Shujing Liu, Congcong Hou, Changjie Dong, Duo Zhao, Quanrui Chen, Jin-Yu Terence Yang, Kai Tang *

State Key Laboratory of Marine Environmental Science, Fujian Key Laboratory of Marine Carbon Sequestration, College of Ocean and Earth Sciences, Xiamen University, China

ARTICLE INFO

Keywords:
Hypoxia
East China sea
Eutrophication
Microbial communities

ABSTRACT

Climate change and eutrophication are accelerating ocean deoxygenation, leading to a global decline in oxygen levels. The East China Sea, frequently experiencing deoxygenation events, harbors diverse microbial communities. However, the response of these communities to the changing deoxygenation dynamics remains poorly understood. Here, we explored the composition and function of microbial communities inhabiting seawaters of the Changjiang Estuary and offshore areas. Our findings suggested that neutral processes significantly influenced the assembly of these communities. The overall bacterial composition demonstrated remarkable high stability across the oxygen gradient. Salinity exhibited a significantly stronger correlation with bacterial community structure than dissolved oxygen. Both metagenomics and metaproteomics revealed that all of the samples exhibited similar functional community structures. Heterotrophic metabolism dominated these sites, as evidenced by a diverse array of transporters and metabolic enzymes for organic matter uptake and utilization, which constituted a significant portion of the expressed proteins. O_2 was the primary electron acceptor in bacteria even under hypoxic conditions, evidenced by expression of low- and high-affinity cytochrome oxidases. Proteins associated with anaerobic processes, such as dissimilatory sulfite reductases, were virtually undetectable. Untargeted liquid chromatography with tandem mass spectrometry analysis of seawater samples revealed a diverse range of dissolved organic matter (DOM) components in amino acids, lipids, organic acids, peptides, and carbohydrates, potentially fueling dominant taxa growth. Despite fluctuations in the abundance of specific genera, the remarkable similarity in community structure, function, and DOM suggests that this ecosystem possesses robust adaptive mechanisms that buffer against abrupt changes, even below the well-defined hypoxic threshold in marine ecosystem.

1. Introduction

Ocean oxygen loss (deoxygenation), listed by IUCN as a primary marine environmental stressor, triggers imbalances in marine life communities (Laffoley et al., 2019). Global warming and enhanced nutrient input due to human activities lead to expansion of deoxygenated zones (Watson et al., 2017). Under the high-emission RCP8.5 scenario, it is projected that a significant majority, exceeding 72%, of the global ocean will witness the emergence of deoxygenation before 2080 (Gong et al., 2021). Deoxygenation of seawater to an dissolved oxygen (DO) concentration below 2 mg/L is defined as hypoxia, because fish and shrimp species normally present on the sea floor are not captured in bottom-dragging trawls at this oxygen levels (Vaquer-Sunyer et al., 2008). Declining oxygen levels affect biogeochemical and biological processes in the oceans, impacting growth, reproduction, and survival of organisms and altering community productivity, biodiversity, and food-web structure (Breitburg et al., 2018). These changes can lead to a loss of ecological services, affecting food security, tourism, and conservation, with fish and shellfish populations particularly vulnerable in hypoxic waters (Levin et al., 2015). Intensifying eutrophication, fueled by anthropogenic nutrient inputs, has led to seasonal hypoxia in the seas around China, including the Changjiang Estuary, Pearl River Estuary, and Bohai Sea (Chen et al., 2007; Luo et al., 2009; Guo et al., 2020). The summer hypoxia zone off the Changjiang Estuary ranks as one of the largest coastal hypoxic systems globally, encompassing an area up to 15, 000 km^2 (Office of integrated oceanographic survey of China, 1961; Lu

* Corresponding author.
E-mail address: tangkai@xmu.edu.cn (K. Tang).

https://doi.org/10.1016/j.envres.2024.119764
Received 6 June 2024; Received in revised form 31 July 2024; Accepted 7 August 2024
Available online 8 August 2024

et al., 2017). Physical stratification and the increased primary production induced by eutrophication, are the key mechanisms controlling this hypoxia (Zhu et al., 2011). The complex water masses, including Changjiang diluted water, Kuroshio subsurface water, and Taiwan warm currents, also affected formation and evolution of hypoxia in the Changjiang Estuary (Zhang et al., 2018).

Falling oxygen levels in the ocean are expected to trigger a shift in ecosystem material and energy flows, with a greater proportion flowing towards lower-level microorganisms rather than higher-level predations (Jessen et al., 2017; Wright et al., 2012). When oxygen concentrations dip below the critical threshold of 20 μM, these areas become designated as oxygen minimum zones (OMZs), with examples found in the coastal Bay of Bengal and the eastern tropical South Pacific (Paulmier et al., 2009). OMZs are recognized as biogeochemical hot spots for denitrification and anammox processes, which play key roles in removing excess nitrogen from the ocean (Ward et al., 2009; Lam et al., 2009; Bertagnolli et al., 2018), and for sulfurization of organic matter, leading to the accumulation of refractory sulfur-rich compounds (Gomez-Saez et al., 2021). The distinct redox gradients (dysoxic 20–90 μM, suboxic 1–20 μM, anoxic <1 μM, and anoxic sulfidic) within OMZs shape a unique microbial landscape, with heterotrophic SAR11 bacteria and anaerobic chemoautotrophs including Thaumarchaeota (dysoxia), SUP05 and sulfur oxidizers (suboxic and anoxic), and Desulphobacteraceae (anoxic sulfidic) (Wright et al., 2012; Pajares et al., 2020; Beman et al., 2021). Research demonstrates that deoxygenation alters microbial communities and their metabolic pathways within OMZs (Bertagnolli et al., 2018; Beman et al., 2013). In contrast to the formation of stable OMZs in other regions, coastal waters around China are relatively shallow, typically less than 100 m deep, and experience seasonal hypoxia. Chinese sea exhibits dynamic and periodic variations in oxygen levels that generally remain well above the suboxic threshold, thus preventing the development of such OMZs. Our understanding of how bacterial community respond to this costal deoxygenation around China remains limited. To address this gap, this study employs high-throughput 16S rRNA sequencing, metagenomics, metaproteomics, and untargeted liquid chromatography with tandem mass spectrometry (LC-MS/MS) to investigate how microbial taxonomic composition, metabolic activities, and DOM respond to hypoxia in the Changjiang Estuary and adjacent East China Sea. The findings of this study will significantly broaden our understanding of the dynamics of microbial communities and their functional variations within changing aquatic ecosystems.

2. Materials and methods

2.1. Sample collection

We conducted a cruise in the Changjiang Estuary and adjacent East China Sea from August 20–30, 2022. Water samples were collected from nine sites, including S01, located in the freshwater of Changjiang Estuary, S02, located in the brackish water, and S03–S09, located in coastal seawater (Fig. 1A). At S01 and S02, only surface water samples were collected, as the minimal vertical gradient in both microbial communities and physicochemical parameters made surface sampling sufficient to represent these sites. At S07 and S08, which located in a submarine basin, samples were collected from the surface, middle, and bottom layers. For the other stations, samples were taken from the surface and bottom layers. The detailed sampling depths were provided in Table S1. About 100 L seawater samples were prefiltered through 3 μm pore-size filters. Filtrates were filtered through 0.2 μm pore-size polycarbonate membranes (142 mm diameter, Millipore) for 16S rRNA gene sequencing, metagenomics, and metaproteomics. After rapidly freezing with liquid nitrogen, the 0.2 μm membranes were stored at −80 °C. For DOM composition analysis, 1 L seawater was filtered through 0.7 μm GFF membrane (47 mm diameter, Whatman), and filtrate was adjusted to pH 2 and extracted through PPL column (200 mg, Bond Elut PPL, Agilent Technologies, USA). Environmental factors including salinity, temperature, depth, chlorophyll *a* (Chl *a*) and DO at each site were measured from a CTD probe (SeaBird Electronics). The concentrations of nitrate (NO_3-N), nitrite (NO_2-N), dissolved inorganic phosphate (DIP), and dissolved inorganic silicate (DISi) were measured using a AA3 Auto-Analyzer (Technicon) (Dai et al., 2008). Cells abundance of picoeukaryotic plankton and bacteria were measured by a flow cytometer (BD Biosciences) (Marie et al., 1999). The concentrations of dissolved organic carbon (DOC) and total dissolved nitrogen (TDN) were analyzed by the Shimadzu TOC-VCPH analyzer. The concentrations of particulate organic carbon (POC) and particulate organic nitrogen (PON) were analyzed on a CHNS elemental analyzer (vario EL cube, Elementar, Germany).

2.2. 16S rRNA gene and metagenomic sequencing

We used 16S rRNA gene and metagenomic sequencing to investigate structure and potential function of bacterial communities in East China Sea. Total microbial genomic DNA was extracted from 0.2 μm membranes using the PowerSoil DNA Isolation Kit (MoBio, Carlsbad, USA). The universal primers "343F" and "798R" was used to amplified V3-V4 region of 16S rRNA gene (Nossa et al., 2010). Amplicons sequencing

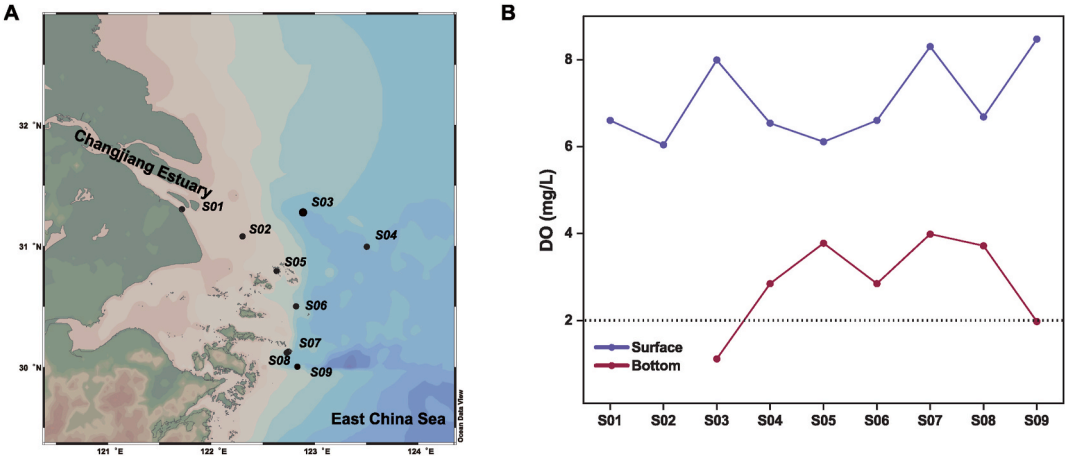

Fig. 1. Sampling sites and DO parameters of hypoxia sites. **A** Location of sampling sites in Changjiang Estuary and adjacent East China Sea. **B** The vertical distribution of DO with water column in sampling sites.

were performed on an Illumina MiSeq platform. Raw 2 × 250 bp paired-end reads were processed using the QIIME 2 v23.2 (Bolyen et al., 2019) to get amplicon sequence variants (ASVs) abundance table and representative sequences. SILVA reference database v138.1 (Yilmaz et al., 2013) was used for taxonomic assignments of ASVs. Metagenomic sequencing was performed on the NovaSeq 6000 sequencing platform at Hanyu Bio-Tech (Shanghai, China). Raw 2 × 150 bp paired-end reads of metagenomics were trimmed to remove adaptors using Trimmomatic v0.36 (Bolger et al., 2014). The clean reads were assembled using Megahit v1.2.2 (Li et al., 2016), and the open reading frames of contigs were predicted using Prodigal v2.6.3 with the parameter -p meta (Hyatt et al., 2010). The number of clean reads aligned on genes was counted using Samtools v1.18 (Li et al., 2009) and the relative abundance of genes was calculated using transcripts per million (TPM). Genes were annotated using DIAMOND v2.0.7 (Buchfink et al., 2015) against the Kyoto Encyclopedia of Genes and Genomes (KEGG) database (Kanehisa et al., 2016).

2.3. Metaproteomics sample analysis and data annotation

We used metaproteomics to investigate the actual metabolic activities and functions that bacteria are performing *in situ*. For protein extraction, the 0.2 μm filters was resuspended in lysis buffer containing 1% protease inhibitor cocktail and 8M urea, and thereafter sonicated on ice using a high intensity ultrasonic processor. Samples were supplemented with urea and dithiothreitol, followed by trypsin digestion. Desalting of the peptide mixture in each sample were conducted by Strata X SPE column. LC-MS/MS analysis was performed on a Q-Exactive™ HF-X (ThermoFisher Scientific) coupled with a EASY-nLC 1200 UPLC system (ThermoFisher Scientific). The mobile phase was composed of a mixture of (A) water contains 0.1% formic acid and 2% acetonitrile and (B) water contains 0.1% formic acid and 90% acetonitrile. The elution gradient was as follows: 0–40 min, gradient from 5% to 22% B; 40–54 min, gradient from 22% to 32% B; 54–57 min, gradient from 32% to 80% B; 57–60 min, isocratic 80% B. The flow rate was set to 500 nL/min. The resulting MS/MS data were searched against gene sets which was generated by metagenomic sequencing using the MaxQuant v.1.6.15.0 (Tyanova et al., 2016). We used the normalized spectral abundance factor (NSAF) values to calculated the relative abundance of proteins (Zybailov et al., 2006). We annotated identified proteins by searching against non-redundant protein sequence database and KEGG database (Kanehisa et al., 2016) using DIAMOND v2.0.7 (Buchfink et al., 2015). Transporters were identified against the transporter classification database (Saier et al., 2021).

2.4. DOM composition analysis by untargeted LC-MS/MS and chemical annotation

PPL columns were eluted with methanol to extract DOM. LC-MS/MS analysis of DOM was performed on a Triple TOF 6600 (AB Sciex) coupled with a 1290 Infinity HPLC (Agilent) in data-dependent acquisition mode (DDA mode). Chromatographic separation was performed using Waters ACQUITY UPLC BEH Amide (2.1 × 100 mm, 1.7 μm) column. The flow rate was set to 0.5 mL/min. The mobile phase was composed of a mixture of (A) 25 mM ammonium acetate with 25 mM ammonia and (B) acetonitrile. The elution gradient was as follows: 0–0.5 min, isocratic 95% B; 0.5–7 min, gradient from 95% to 65% B; 7–8 min, gradient from 65% to 40% B; 8–9 min, isocratic 40% B; 9–9.1 min, gradient from 40% to 90% B; 9.1–12 min, isocratic 95% B. MS^1 scans were acquired in the positive mode with the m/z 50–1000 range. The twelve most abundant precursors per MS^1 spectra were then selected for fragmentation to acquire MS^2 data.

Metabolomics analysis followed standardized LC-MS/MS data processing by Earth Microbiome Project (Shaffer et al., 2022). LC-MS/MS raw data were converted to mzML open format using ProteoWizard v3.0.19 (Chambers et al., 2012). The mzML files were processed with MZmine v2.5.3 to detect feature peak (Pluskal et al., 2010). Peak areas and spectral information of each feature were exported to the Global Natural Products Social Molecular Networking (GNPS) for molecular networking (Wang et al., 2016). And SIRIUS v4.0.1 was used to systematically complete compound annotations (Duhrkop et al., 2019). Molecular formula was computed with SIRIUS v4.0.1 and refined with ZODIAC module (Ludwig et al., 2020). Structure annotation was done with CSI:FingerID module (Duhrkop et al., 2015). Chemical class annotations were conducted with CANOPUS module (Duhrkop et al., 2021) according to the ClassyFire ontology (Feunang et al., 2016).

2.5. Data analysis

The alpha-diversity and Bray-Curtis similarity matrix of microbial communities and DOM features were calculated in R language (R Core Team, 2022). Mantel tests was used to reveal correlations between environmental factors and bacterial community, protein expression or DOM features, respectively. The relative importance of stochastic processes on bacterial community assembly was calculated using neutral community model (NCM) (Hubbell, 2001; Chen et al., 2019). Distance-decay relationships was accessed by linear regression analysis between the Bray-Curtis dissimilarity and geographical distances.

3. Results

3.1. Environmental parameters

Sampling stations exhibited high degrees of heterogeneities in salinity and DO concentrations (Table S1). Salinity varied considerably, ranging from 0.64‰ in the surface layer at station S01 to 34.38‰ in the bottom layer at station S04. DO concentrations ranged from to 3.99 to 1.12 mg/L in the bottom water, indicating the presence of deoxygenated environments (Fig. 1). In the bottom layers of S03 and S09, dissolved oxygen levels are even below 2 mg/L (Fig. 1). Chl α values ranged from 0.11 g/m^3 (S04 bottom) to 17.21 g/m^3 (S09 surface). Total prokaryotic abundance ranged from 9.38×10^5 cell/mL (S05 bottom) to 9.95×10^6 cell/mL (brackish water). The surface layer of freshwater exhibited the highest DOC concentration, reaching 150 μM, while the bottom layer of station S06 showed the lowest point value at 87 μM. The ranges of TDN, POC, and PON concentration were 9.1–73.6 μM, 10.2–54.5 μM, and 1.5–8.2 μM, respectively.

3.2. Bacterial community composition in Changjiang Estuary and adjacent East China sea

The bacterial community composition, visualized at the order level in Fig. 2A, consisted of 1,806 ASVs identified from 27 phyla. Proteobacteria (71.97%), Bacteroidota (13.59%), Actinobacteriota (9.72%), and Cyanobacteria (1.39%) dominated these bacterial communities (Fig. S1A). Within the Proteobacteria, Alphaproteobacteria emerged as the most abundant class, followed by the Gammaproteobacteria (Fig. 2A). A clear stratified variation in bacterioplankton communities was observed (Fig. 2A). Freshwater station S01 harbored significantly higher proportions of Burkholderiales and Actinobacteriota compared to marine stations. At S01, the majority of Actibobacteriota ASVs belonged to the hgcI clade and CL500-29 marine group. *Nocardioides* was a dominant genus within the Actinobacteriota phylum at S02, while *Candidatus Actinomarina* and Sva0996 marine group were dominant within Actinobacteriota at other seawater stations (Table S2). The relative proportion of SAR11 increased significantly from surface to bottom water ($p < 0.01$), ranging from 1.7% in surface of brackish site to 36.9% in bottom of S07. While freshwater SAR11 at station S01 belonged to freshwater lineage IIIb subclade (Fig. S1), seawater stations across the sampling area harbored Ia subclade, the dominant marine SAR11 group, as the predominant subtype. The relative proportion of Rhodobacterales decreased significantly from surface to bottom water

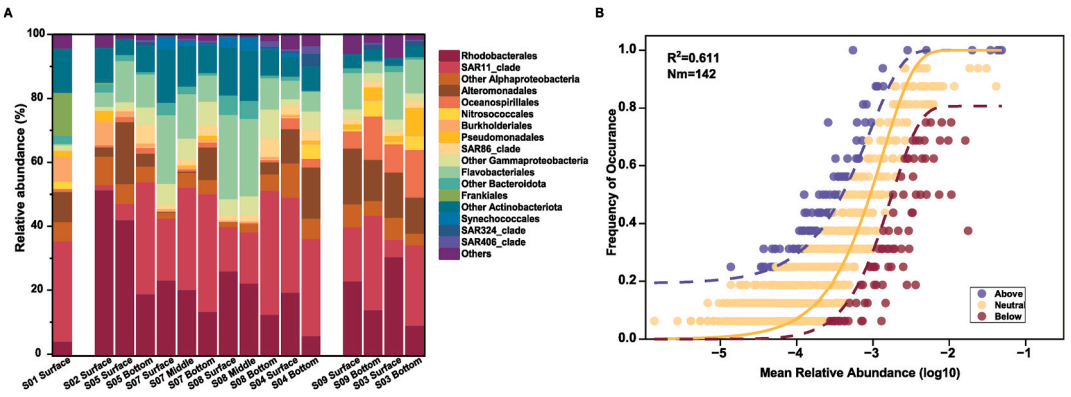

Fig. 2. The structure and assembly process of bacterial communities. **A** Relative abundances of bacterial communities at the order level. **B** The predicted occurrence frequencies for bacterial communities in Changjiang Estuary and adjacent East China Sea. The solid yellow line is the best fit to NCM, and the dashed line indicates 95% confidence intervals around the NCM prediction. ASVs that occur more or less frequently than predicted by the NCM are shown in purple and red, respectively. R^2 represents the fit to this model.

($p < 0.01$). Within Rhodobacterales, the dominant genus shifted from *Sagittula* in freshwater sites to *Salipiger* and *Aliishimia* in seawater (Table S2). Flavobacteriaceae within Bacteroidetes (3.51–26.35% in seawater) were dramatically more abundant compared to freshwater (0.43%). The relative abundance of Alteromonadales varies greatly across stations and depths. In S07 and S08, surface and middle layers show a meager presence of Alteromonadales, ranging from 0.05% to 0.23%. In contrast, other stations exhibited a significantly higher abundance, reaching up to 19.37%. Despite their low prevalence, gammaproteobacterial SAR324, SUP05, SAR86, and UBA10353, showed a slight preference for the bottom water. Nitrite-oxidizing bacteria of Nitrospinota and Nitrospirota were found in the bottom seawater, only accounting for 0.01% and 0.009%, respectively. The relative abundance of Oceanospirillales ranged from 0.18% to 14.92%, peaking in the bottom layers of S09 and S03, with the values of 13.57 and 14.92%, respectively (Table S2).

3.3. Functional pattern of microbial communities in Changjiang Estuary and adjacent East China sea

Potential and expressed functions displayed remarkably consistent functional structures across all samples (Fig. 3, Fig. S2). Metaproteomics identified a diverse array of transporters for organic compounds including amino acids, peptides, organic acids, lipids, and carbohydrates, indicative of active heterotrophy in coastal waters (Fig. 4). Membrane transporters, primarily contributed by Rhodobacterales, accounted for 23.9–32.7% of the East China Sea metaprotemics, with proteins involved in amino acid, lipid, carbohydrate, glycan, and nucleotide metabolism forming a major part (Table S3). The identification of cytochrome oxidases, enzymes that catalyze the terminal electron transfer during oxygen respiration, provided further evidence for active aerobic respiration (Fig. S3). While low-affinity cytochrome *c* oxidases were prevalent, high-affinity cytochrome bd and cbb3 oxidases were also expressed in the transition from oxygenated to deoxygenated water (Fig. S3). Spearman correlation analysis revealed decrease of oxygen concentration did not significantly increase the expression of low- and high-affinity cytochrome oxidases ($p > 0.05$). This suggests that aerobic metabolism and heterotrophic activity still dominated in deoxygenated zones.

Through metaproteomic analysis, we also identified pathway components driving carbon and energy metabolism in carbon fixation, nitrification, anammox, and denitrification. In the bottom deoxygenated water, 3-hydroxypropionate dehydrogenase, a marker for the 3-hydroxypropionate/4-hydroxybutyrate cycle, originated solely from Thaumarchaeota (Fig. 4). While proteins associated with the Calvin-Benson-Bassham (CBB) cycle, primarily from Synechococcales, declined, those involved in the reverse TCA cycle increased. Notably, proteins for nitrification, including Thaumarchaeota-derived ammonia monooxygenase subunits (Amo) and Nitrospinota/Planctomycetota-derived nitrite oxidase (NXR), exhibited higher NSAF in the bottom deoxygenated water. Similarly, NSAF values for dissimilatory nitrate reductase (Nar) involved in partial denitrification also increased. Anammox

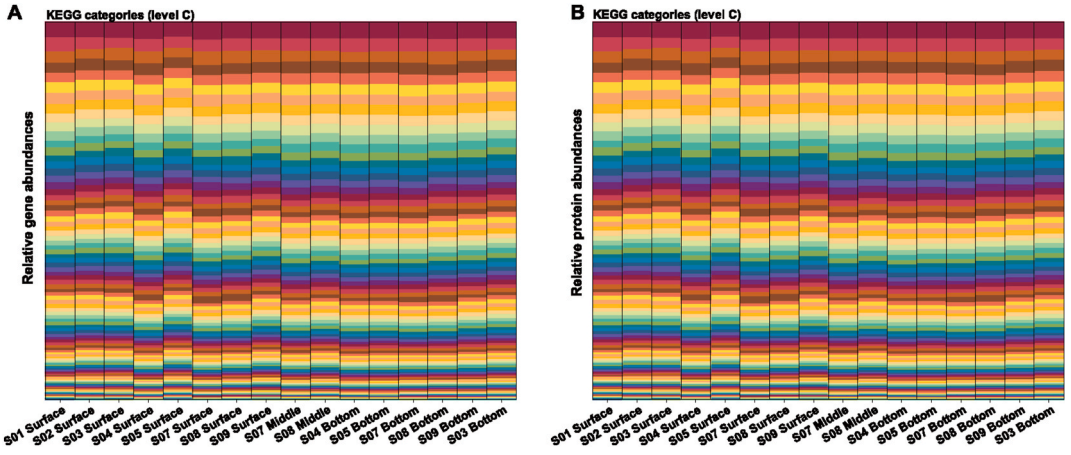

Fig. 3. Potential and expressed functions of microbial communities. Corresponding metagenomic (A) and metaproteomic (B) community composition based on KEGG Level C categories (one column per sample, one colour per gene group). For details on functional genes and proteins, see supplementary Table S3 and Table S4.

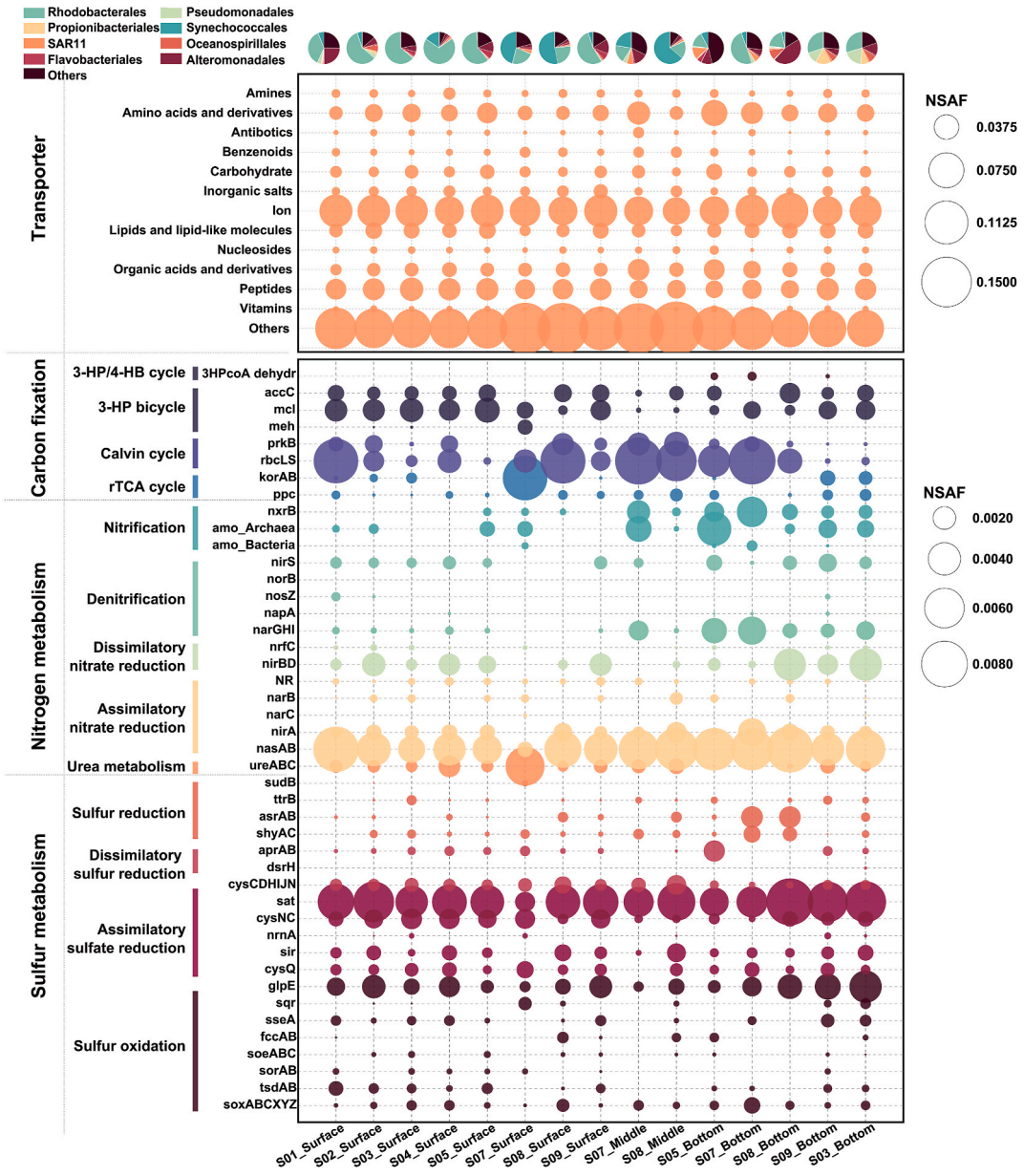

Fig. 4. The relative abundance of transporters and selected core proteins that involved carbon, nitrogen, and sulfur metabolism in the metaproteomics. 3HP/4HB, 3-hydroxypropionate/4-hydroxybutyrate; 3-HP bicycle, 3-hydroxypropionate bicycle; 3HPcoA dehydr, 3-hydroxypropionyl-coenzyme A dehydratase; accC, acetyl-CoA carboxylase; mcl, malyl-CoA/(S)-citramalyl-CoA lyase; meh, 3-methylfumaryl-CoA hydratase; prkB, phosphoribulokinase; rbcLS, ribulose-bisphosphate carboxylase; korAB, 2-oxoacid ferredoxin oxidoreductase; ppc, PEP carboxylase; nxrB, nitrite oxidoreductase; amo, ammonia monooxygenase; nirS, nitrite reductase; norB, nitric oxide reductase; nosZ, nitrous-oxide reductase; napA, periplasmic nitrate reductase; narGHI, dissimilatory nitrate reductase; nrfC, cytochrome *c* nitrite reductase Fe-S; nirBD, nitrite reductase; NR, nitrate reductase; nar, assimilatory nitrate reductase; nirA, ferredoxin-nitrite reductase; nasAB, assimilatory nitrate reductase; ureAB, urease; sudB, sulfide dehydrogenase; ttrB, tetrathionate reductase; asrAB, anaerobic sulfite reductase; shyAC, sulfhydrogenase; aprAB, adenylylsulfate reductase; dsrH cysCDHIJN, assimilatory sulfate reduction; sat, Sulfate adenylyltransferase; cysNC, bifunctional enzyme CysN and CysC; nrnA, bifunctional oligoribonuclease and PAP phosphatase; sir, sulfite reductase; cysQ, PAPS phosphatase; glpE, sqr, sseA, fccAB, soeABC, sulfite dehydrogenase; sorAB, sulfur oxygenase; tsdAB, thiosulfate dehydrogenase; soxABCXYZ, sox multienzyme system. The circles representing NSAF values provide relative peptide abundances in each protein. For details on functional proteins, see Supplementary Table S4.

protein signatures were undetectable across all the samples.

Across the investigated sites, protein KO abundances revealed high functional redundancy, independent of distance (slope = 0.003, $p > 0.05$) (Fig. 5B). Principal coordinates analysis (PCoA) revealed no significant difference in protein expression profiles across samples (Fig. 5A). Functional compositions of metaproteomics did not significantly correlate with these environmental factors, as shown by Mantel tests (Fig. 6). The taxonomic composition of the metaproteomics exhibited a significant and strong correlation with oxygen level (Fig. 6). This suggests that while microbial functions remain conserved despite DO variation, and hypoxia alters the relative contribution of different microorganisms to those function.

3.4. DOM diversity based on LC-MS/MS analysis

Given the intricate relationship between DOM and microorganisms, we employed untargeted LC-MS/MS to analyze the DOM composition in these water bodies. Our analysis revealed a rich diversity of organic molecules, with 590 unique molecular features identified. Further characterization through MS/MS spectra comparisons with GNPS

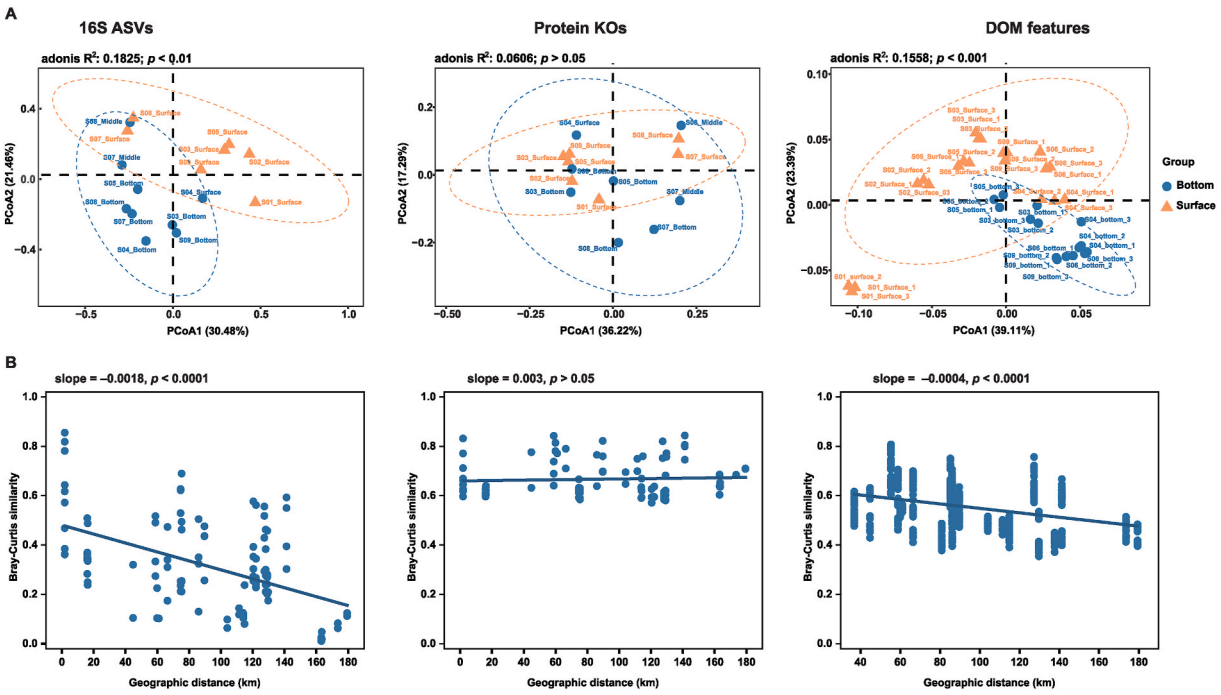

Fig. 5. Principal coordinates analysis (A) and distance-decay patterns (B) based on the Bray-Curtis similarity of bacterial communities, expressed proteins, and DOM features. Solid lines denote the least squares linear regression across spatial scales.

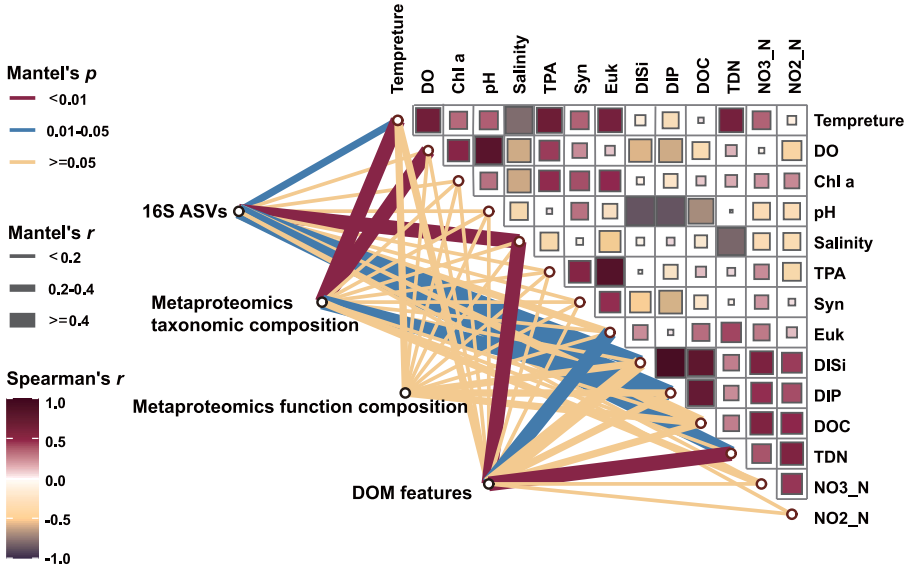

Fig. 6. Environmental drivers of bacterial communities, metaproteomic taxonomy composition, metaproteomic function composition, and DOM features. Pairwise comparisons of environmental factors are shown at the upper-right, with a color gradient representing Spearman's correlation coefficients. Microeukaryotic plankton community composition was correlated to each environmental factor by Mantel tests. The line width represents the partial Mantel's r statistic for the corresponding correlation, and line color means that significance is tested based on 999 permutations. DO, dissolved oxygen; Chl-a, chlorophyll-a; TPA, total prokaryotic abundance; Syn, synechococcus abundance; Euk, heterotrophic eukaryotic abundance (<20 μm); DISi, dissolved silicate; DIP, dissolved inorganic phosphate; DON, dissolved organic carbon; TDN, total dissolved nitrogen; NO3-N, nitrate nitrogen; NO2-N, nitrite nitrogen.

database enabled the annotation of 103 known features within this complex mixture. We identified the major classes of DOM features, including amino acids, lipids, peptides, and carbohydrates. The absolute intensities of DOM features categories in the surface layer were significantly higher than those of bottom layer ($p < 0.01$), with the exception for lipids and lipid-like molecules (Fig. 7B). It is expected due to the higher DOC concentrations in surface layer (Table S1). Considering both the identity and relative intensity of individual DOM features, hierarchical clustering of Bray-Curtis calculated on these features revealed a clear separation among freshwater, seawater surface, and seawater bottom samples (Fig. 7A). We found high Bray-Curtis similarity in DOM feature composition across sites, demonstrating a significant but shallower distance effect compared to taxonomic composition (slope = −0.0004, $p < 0.0001$) (Fig. 5). Mantel tests revealed significant correlations between DOM features composition and salinity, TDN, and cell abundance of eukaryotic phytoplankton (Fig. 6). The significant correlations between DOM features and salinity indicated that the DOM in this region originate from the river and riverine nutrients likely

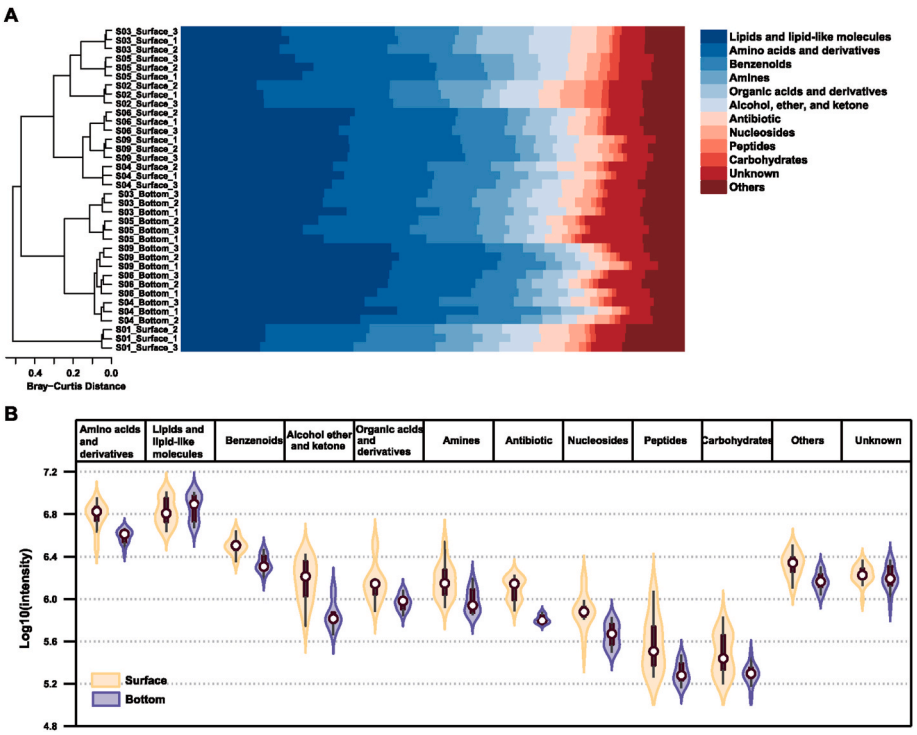

Fig. 7. Distribution of DOM features superclasses detected by untargeted LC-MS/MS among samples. Chemical superclass annotations are shown relative intensities (**A**) and absolute intensities (**B**) of molecular features.

undergoing conservative degradation during the long-range transport from the river mouth.

Mantel tests revealed strong correlations between the composition of DOM features and 16S rRNA gene ASVs (Pearson's $r = 0.62$, $p < 0.001$). As the main substrate and energy source for heterotrophic bacterioplankton, DOM composition directly influenced microbial community structure. Notably, amino acids and derivatives, and peptides exhibited the highest absolute and relative intensities at the S02 site (Fig. 7B). These readily consumed substrates likely fueled the dominance of Roseobacteraceae at S02, where they comprised 44.4% of the community, far exceeding other stations (Fig. S1). While our analysis did not reveal significant correlations between DOM features and metaproteomic function based on KO abundances (Pearson's $r = 0.27$, $p > 0.05$), potentially due to functional redundancy. The integration of metaproteomics and LC-MS/MS datasets provide opportunities to link substrates to their associated enzymes. A diverse array of transporters and metabolic enzymes crucial for organic matter uptake and utilization constituted a major portion of the expressed proteins (Table S3). For instance, except in S07 and S08 where LC-MS/MS sampling was absent, feature15, annotated by GNPS as galactarate with the $m/z = 228.1964$ $[M+H]^+$, was detected with high intensities in all other samples (Table S4). Meanwhile, expression of galactarate dehydratase was also identified in most samples (Table S3). Feature513, annotated by GNPS as gallate with the $m/z = 171.0654$ $[M+H]^+$, exhibited high intensity only in the surface water of the S03 site (Table S4). Within the metaproteomics, only gallate dioxygenase was identified, suggesting its role in metabolizing this compound primarily by Alteromonadaceae at the S03 site (Table S3). This finding supports the notion that DOM, as a source of carbon and energy source, sustains the heterotrophic life of microbial communities in the Changjiang Estuary and adjacent East China Sea.

4. Discussion

A fascinating shift at the family level occurred from the Changjiang Estuary to offshore (Fig. S1). Mantel tests revealed that, among all measured parameters, salinity had the strongest correlations with bacterial community composition (Fig. 6). Other significant environmental variables were temperature, DISi, DIP, and TDN (Fig. 6). This was consistent with previous survey that revealed significant influence of the nutrient concentrations and temperature on bacterial composition (Wang et al., 2015). It should be noted that DO showed no significant correlation with bacterial community composition in our analysis (Fig. 6). Despite the occurrence of deoxygenation, opportunistic members of the Rhodobacterales, Flavobacteriales, and Ateromonadales, along with the oligotrophic SAR11 clade were recognized as the dominating clades and together represented approximately 65% of all bacteria present in East China Sea (Fig. 2a). SAR11 demonstrates a competitive advantage in resource acquisition, facilitated by cell size reduction, minimized replication costs, and maximized transport functions (Giovannoni, 2017). Rhodobacterales, Flavobacteriales, and Alteromonadales exhibit specialization in the processing of low-molecular-weight phytoplankton-derived metabolites, high-molecular-weight carbohydrate polymers, and both classes, respectively, contributing to their dominance in coastal ecosystems (Landa et al., 2017; Avcı et al., 2020; Pedler et al., 2014). The relative abundance of these dominant taxa varies independently of dissolved oxygen levels, even within the Bohai Sea's seasonal hypoxic zones (Wu et al., 2022). Furthermore, consistent with observations in the Changjiang Estuary, correlation coefficient analysis in the Pearl River Estuary demonstrated that salinity exhibits a greater influence on the structural organization of microbial communities compared to dissolved oxygen (Chen et al., 2021). A previous study proposed that both selection processes, acting on specific bacterial characteristics, and neutral processes, driven by random chance events, jointly govern the assembly and biogeographical patterns of bacterial communities in subtropical bays of China (Mo et al., 2018). The neutral theory considers that microbial communities exhibiting a balance between the speciation and extinction of taxa, was shaped by stochastic processes, which involve random death, speciation, and dispersal, shape the microbial community structure (Hubbell, 2001; Chen et al., 2019). Even under hypoxia's pressure, neutral processes remain the primary drivers of community structure

(Fig. 2b). Our NCM successfully explained a large fraction ($R^2 = 61.1\%$) of the entire bacterial community assembly, indicating that neutral processes play a strong role for shaping the community structure in this area (Fig. 2b). Null model analysis also confirmed that dispersal limitation (62.2%) and undominated (37.8%) were dominant in assembly of these communities. The significantly observed distance-decay pattern of bacterial communities from estuary to offshore further confirmed the importance of stochastic processes (Fig. 5b). This finding likely arises from the complex hydrological environment of the Changjiang Estuary where mixing occurs between the Changjiang River freshwater, the Taiwan Warm Current, and the Yellow Sea coastal water (Chen et al., 1999). Faster water flow in this mix could facilitate high levels of microbial dispersal (Chen et al., 2019). The majority ASVs belonging to SAR11 and opportunistic taxa had a good fit to the neutral partition (Fig. 2b). This pattern might explain the wide distribution observed for these dominant groups.

Our metagenomic and metaproteomic analysis showed a relative uniform in functional composition across samples, suggesting heterotrophic dominance in the East China Sea (Fig. 3). Bacteria in the investigated areas primarily used oxygen as an electron acceptor, contrasting with the usage of alternative terminal electron acceptors in OMZs, such as NO^{3-}, NO^{2-}, manganese, iron, sulfate, and CO_2 (Ulloa et al., 2012; Hawley et al., 2014). Despite high variation in ASVs, functional dissimilarity across communities remains lower due to the sharing of metabolic functions by taxonomically distinct microorganisms (Louca et al., 2018). Our untargeted LC-MS/MS analysis showed that DOM compositions from hypoxic water did not cluster separately, and the distance-decay patterns indicated greater variation in DOM features across sampling distances compared to those induced by hypoxia (Fig. 5). Freshwater sites exhibited high intensities of non-biogenic substances (e.g., delphene and 4-acetamidoantipyrine) and higher plant-derived compounds (e.g., rhodojaponin VI) compared to seawater, as detailed in Table S4. Eutrophication-driven algal blooms are considered as the primary driver for expanded hypoxia in coastal oceans, such as the Changjiang Estuary and its adjacent East China Sea (Chen et al., 2007; Jiang et al., 2010; Zhu et al., 2017). Elevated primary production and intense stratification can lead to oxygen depletion in near-bottom waters (Zhu et al., 2011). Surface phytoplankton blooms contribute to an enhanced vertical flux of organic matter to bottom waters for bacterial respiration (Zhang et al., 2010). But we investigated that DOC concentrations remained relatively stable at hypoxia sites (Table S1). The collective evidence from functional proteins expression and DOM feature composition suggested that the microbial community maintains a primarily heterotrophic lifestyle in the deoxygenated zone of East China Sea.

Aerobic microorganisms still dominated the microbial communities in China Sea even in the event of deoxygenation. Facultatively anaerobic microorganisms such as SUP05 were present in both surface and bottom layers across our investigated areas, but their abundance and protein expression remained low (Table S2). Compared to benthic organisms vulnerable to hypoxia, bacteria can still survive even at low-nanomolar oxygen levels (Zakem et al., 2017). Microbial aerobic respiration exhibited the adaptation to low oxygen environments, which expands the number of available ecological niches (Han et al., 2011). About 70% of bacteria genomes contain gene coding high-affinity cytochrome oxidases, allowing them to access to scarce oxygen supplies (Morris et al., 2013). And no significant relationship between oxygen level and cytochrome oxidases was observed in our studies areas (Fig. S3). Furthermore, phytoplankton continues to produce DOM in hypoxia zones, providing a carbon source for bacterial oxygen consumption and thereby sustaining the hypoxic conditions (Zhang et al., 2010). Generally, 20 μM O_2 is considered the threshold value of dissolved oxygen concentrations for traditional denitrification (Lam et al., 2011). We observed proteins for partial denitrification in both surface and bottom layers of our samples, while oxygen concentration did not significantly affect the expression levels of nirs for denitrification (Fig. 4). Particle-associated denitrification is hot spots of nitrogen cycling in oxic coastal waters, independent of hypoxia (Wan et al., 2023). Hypoxia and acidification often co-occur, as microbial decomposition depletes oxygen and releases carbon dioxide. The pH of seawater decreases as the concentration of DO decreases in our samples (Table S1). However, bacterial communities in coastal ecosystems also exhibited adaptation to a short-term reduction in the pH which induced by elevated pCO_2 (Yang et al., 2021). Thresholds represent the limit or tolerance range at which an ecosystem withstands external disturbances, causing a state change in response to external environmental changes and exhibiting entirely distinct characteristics in this system (Egidi et al., 2023). When the oceans deoxygenate to an oxygen concentration of 2 mg/L, fisheries collapse, yet the transition into oxygen-deficient conditions is not an abrupt change for the microbial ecosystem. This study provides valuable insights into the microbial community structure and function during a one-off sampling event over a duration of 10 days. However, long-term and multi-seasonal studies are needed to confirm these findings and provide a more comprehensive understanding of the microbial community dynamics in the Changjiang Estuary and adjacent East China Sea.

5. Conclusion

Neutral processes significantly shape bacterial communities in the Changjiang Estuary and adjacent East China Sea, dominated by opportunistic members of Rhodobacterales, Flavobacteriales, Alteromonadales, and the oligotrophic SAR11 clade. Despite the presence of deoxygenation, the expression of proteins and the availability of DOM support a heterotrophic lifestyle and aerobic respiration. This suggests that, rather than experiencing abrupt changes, microbial communities adapt to deoxygenated conditions. Notably, deoxygenation to 2 mg/L, does not appear to trigger sudden shifts in community composition.

CRediT authorship contribution statement

Shujing Liu: Writing – review & editing, Writing – original draft, Visualization, Methodology, Investigation, Formal analysis, Data curation. **Congcong Hou:** Writing – review & editing, Methodology, Investigation. **Changjie Dong:** Writing – review & editing, Methodology, Investigation. **Duo Zhao:** Writing – review & editing, Methodology, Formal analysis. **Quanrui Chen:** Writing – review & editing, Methodology, Investigation. **Jin-Yu Terence Yang:** Writing – review & editing, Investigation. **Kai Tang:** Writing – review & editing, Writing – original draft, Supervision, Resources, Project administration, Funding acquisition, Conceptualization.

Declaration of competing interest

The authors declare that they have no known competing financial interests or personal relationships that could have appeared to influence the work reported in this paper.

Data availability

16S rRNA, metagenomics, metaproteomics and untargeted LC-MS/MS raw data have been uploaded to the National Omics Data Encyclopedia (NODE, https://www.biosino.org/node/) database with the identifier OEX024197, OEX024198, OEX027023, and OEX027035, respectively.

Acknowledgments

This study was supported by the National Key Research and Development Program of China (2020YFA0608300), the National Natural Science Foundation of China project (92251306, 42076160, 42188102).

Appendix A. Supplementary data

Supplementary data to this article can be found online at https://doi.org/10.1016/j.envres.2024.119764.

References

Avcı, B., et al., 2020. Polysaccharide niche partitioning of distinct Polaribacter clades during North Sea spring algal blooms. ISME J. 14 (6), 1369–1383.

Beman, J.M., Carolan, M.T., 2013. Deoxygenation alters bacterial diversity and community composition in the ocean's largest oxygen minimum zone. Nat. Commun. 4, 2705.

Beman, J.M., et al., 2021. Biogeochemistry and hydrography shape microbial community assembly and activity in the eastern tropical North Pacific Ocean oxygen minimum zone. Environ. Microbiol. 23 (6), 2765–2781.

Bertagnolli, A.D., Stewart, F.J., 2018. Microbial niches in marine oxygen minimum zones. Nat. Rev. Microbiol. 16 (12), 723–729.

Bolger, A.M., Lohse, M., Usadel, B., 2014. Trimmomatic: a flexible trimmer for Illumina sequence data. Bioinformatics 30 (15), 2114–2120.

Bolyen, E., et al., 2019. Reproducible, interactive, scalable and extensible microbiome data science using QIIME 2. Nat. Biotechnol. 37 (8), 852–857.

Breitburg, D., et al., 2018. Declining oxygen in the global ocean and coastal waters. Science 359 (6371), eaam7240.

Buchfink, B., Xie, C., Huson, D.H., 2015. Fast and sensitive protein alignment using DIAMOND. Nat. Methods 12 (1), 59–60.

Chambers, M.C., et al., 2012. A cross-platform toolkit for mass spectrometry and proteomics. Nat. Biotechnol. 30 (10), 918–920.

Chen, J., et al., 1999. The processes of dynamic sedimentation in the Changjiang Estuary. J. Sea Res. 41 (1), 129–140.

Chen, C.-C., Gong, G.-C., Shiah, F.-K., 2007. Hypoxia in the East China Sea: one of the largest coastal low-oxygen areas in the world. Mar. Environ. Res. 64 (4), 399–408.

Chen, W., et al., 2019. Stochastic processes shape microeukaryotic community assembly in a subtropical river across wet and dry seasons. Microbiome 7 (1), 138.

Chen, F., et al., 2021. Microbiological assessment of ecological status in the Pearl River Estuary, China. Ecol. Indicat. 130, 108084.

Dai, M., et al., 2008. Nitrification and inorganic nitrogen distribution in a large perturbed river/estuarine system: the Pearl River Estuary, China. Biogeosciences 5 (5), 1227–1244.

Duhrkop, K., et al., 2015. Searching molecular structure databases with tandem mass spectra using CSI:FingerID. Proc. Natl. Acad. Sci. U.S.A. 112 (41), 12580–12585.

Duhrkop, K., et al., 2019. Sirius 4: a rapid tool for turning tandem mass spectra into metabolite structure information. Nat. Methods 16 (4), 299–302.

Duhrkop, K., et al., 2021. Systematic classification of unknown metabolites using high-resolution fragmentation mass spectra. Nat. Biotechnol. 39 (4), 462–471.

Egidi, E., et al., 2023. Assessing critical thresholds in terrestrial microbiomes. Nat. Microbiol. 8 (12), 2230–2233.

Feunang, Y.D., et al., 2016. ClassyFire: automated chemical classification with a comprehensive, computable taxonomy. J. Cheminformat. 8, 61.

Giovannoni, S.J., 2017. SAR11 bacteria: the most abundant plankton in the oceans. Ann. Rev. Mar. Sci 9 (1), 231–255.

Gomez-Saez, G.V., et al., 2021. Sulfurization of dissolved organic matter in the anoxic water column of the Black Sea. Sci. Adv. 7 (25), eabf6199.

Gong, H.J., Li, C., Zhou, Y.T., 2021. Emerging global ocean deoxygenation across the 21st century. Geophys. Res. Lett. 48 (23). , e2021GL095370.

Guo, J., et al., 2020. Hypoxia, acidification and nutrient accumulation in the Yellow Sea cold water of the South Yellow Sea. Sci. Total Environ. 745, 141050.

Han, H., et al., 2011. Adaptation of aerobic respiration to low O_2 environments. Proc. Natl. Acad. Sci. U.S.A 108 (34), 14109–14114.

Hawley, A.K., et al., 2014. Metaproteomics reveals differential modes of metabolic coupling among ubiquitous oxygen minimum zone microbes. Proc. Natl. Acad. Sci. U.S.A. 111 (31), 11395–11400.

Hubbell, S.P., 2001. A Unified Neutral Theory of Biodiversity and Biogeography. Princeton University Press.

Hyatt, D., et al., 2010. Prodigal: prokaryotic gene recognition and translation initiation site identification. BMC Bioinform. 11 (8), 119.

Jessen, G.L., et al., 2017. Hypoxia causes preservation of labile organic matter and changes seafloor microbial community composition (Black Sea). Sci. Adv. 3 (2), e1601897.

Jiang, T., et al., 2010. Long-term ecological interactions between nutrient and phytoplankton community in the Changjiang estuary. Chin. J. Oceanol. Limnol. 28 (4), 887–898.

Kanehisa, M., et al., 2016. KEGG as a reference resource for gene and protein annotation. Nucleic Acids Res. 44 (D1), D457–D462.

Laffoley, D., Baxter, J., 2019. Ocean Deoxygenation: Everyone's Problem. Causes, Impacts, Consequences and Solution. International Union for Conservation of Nature (IUCN).

Lam, P., et al., 2009. Revising the nitrogen cycle in the Peruvian oxygen minimum zone. Proc. Natl. Acad. Sci. U.S.A. 106 (12), 4752–4757.

Lam, P., Kuypers, M.M.M., 2011. Microbial nitrogen cycling processes in oxygen minimum zones. Ann. Rev. Mar. Sci 3 (1), 317–345.

Landa, M., et al., 2017. Bacterial transcriptome remodeling during sequential co-culture with a marine dinoflagellate and diatom. ISME J. 11 (12), 2677–2690.

Levin, L.A., Breitburg, D.L., 2015. Linking coasts and seas to address ocean deoxygenation. Nat. Clim. Change 5 (5), 401–403.

Li, H., et al., 2009. The sequence alignment/map format and SAMtools. Bioinformatics 25 (16), 2078–2079.

Li, D., et al., 2016. MEGAHIT v1.0: a fast and scalable metagenome assembler driven by advanced methodologies and community practices. Methods 102, 3–11.

Louca, S., et al., 2018. Function and functional redundancy in microbial systems. Nat. Ecol. Evol. 2 (6), 936–943.

Lu, W.H., et al., 2017. The temporal-spatial distribution and changes of dissolved oxygen in the Changjiang Estuary and its adjacent waters for the last 50 a. Acta Oceanol. Sin. 36 (5), 90–98.

Ludwig, M., et al., 2020. Database-independent molecular formula annotation using Gibbs sampling through ZODIAC. Nat. Mach. Intell. 2 (11), 629–641.

Luo, L., Li, S., Wang, D., 2009. Hypoxia in the Pearl River Estuary, the South China sea, in july 1999. Aquat. Ecosys. Health Manag. 12 (4), 418–428.

Marie, D., et al., 1999. Enumeration of phytoplankton, bacteria, and viruses in marine samples. Curr. Protoc. Cytom. 10 (1), 11.11.1–11.11.15.

Mo, Y., et al., 2018. Biogeographic patterns of abundant and rare bacterioplankton in three subtropical bays resulting from selective and neutral processes. ISME J. 12 (9), 2198–2210.

Morris, R.L., Schmidt, T.M., 2013. Shallow breathing: bacterial life at low O2. Nat. Rev. Microbiol. 11 (3), 205–212.

Nossa, C., et al., 2010. Design of 16S rRNA gene primers for 454 pyrosequencing of the human foregut microbiome. World J. Gastroenterol. 16 (33), 4135–4144.

Office of integrated oceanographic survey of China, 1961. Dataset of the national integrated oceanographic survey. In: Survey Data of Hydrometeorological and Chemical Elements in the Bohai, Huanghai and East China Seas. Beijing.

Pajares, S., Varona-Cordero, F., Hernandez-Becerril, D.U., 2020. Spatial distribution patterns of bacterioplankton in the oxygen minimum zone of the tropical Mexican Pacific. Microb. Ecol. 80 (3), 519–536.

Paulmier, A., Ruiz-Pino, D., 2009. Oxygen minimum zones (OMZs) in the modern ocean. Prog. Oceanogr. 80 (3–4), 113–128.

Pedler, B.E., Aluwihare, L.I., Azam, F., 2014. Single bacterial strain capable of significant contribution to carbon cycling in the surface ocean. Proc. Natl. Acad. Sci. U.S.A. 111 (20), 7202–7207.

Pluskal, T., et al., 2010. MZmine 2: modular framework for processing, visualizing, and analyzing mass spectrometry-based molecular profile data. BMC Bioinform. 11 (1), 395.

R Core Team, 2022. R: A Language and Environment for Statistical Computing. R Foundation for Statistical Computing, Vienna, Austria.

Saier, M.H., et al., 2021. The transporter classification database (TCDB): 2021 update. Nucleic Acids Res. 49 (D1), D461–d467.

Shaffer, J.P., et al., 2022. Standardized multi-omics of Earth's microbiomes reveals microbial and metabolite diversity. Nat. Microbiol. 7 (12), 2128–2150.

Tyanova, S., Temu, T., Cox, J., 2016. The MaxQuant computational platform for mass spectrometry-based shotgun proteomics. Nat. Protoc. 11 (12), 2301–2319.

Ulloa, O., et al., 2012. Microbial oceanography of anoxic oxygen minimum zones. Proc. Natl. Acad. Sci. U.S.A. 109 (40), 15996–16003.

Vaquer-Sunyer, R., Duarte, C.M., 2008. Thresholds of hypoxia for marine biodiversity. Proc. Natl. Acad. Sci. U.S.A. 105 (40), 15452–15457.

Wan, X.S., et al., 2023. Particle-associated denitrification is the primary source of N_2O in oxic coastal waters. Nat. Commun. 14 (1), 8280.

Wang, Y., et al., 2015. Spatiotemporal dynamics and determinants of planktonic bacterial and microeukaryotic communities in a Chinese subtropical river. Appl. Microbiol. Biotechnol. 99 (21), 9255–9266.

Wang, M.X., et al., 2016. Sharing and community curation of mass spectrometry data with global natural Products social molecular networking. Nat. Biotechnol. 34 (8), 828–837.

Ward, B.B., et al., 2009. Denitrification as the dominant nitrogen loss process in the Arabian Sea. Nature 461 (7260), 78–81.

Watson, A.J., Lenton, T.M., Mills, B.J.W., 2017. Ocean deoxygenation, the global phosphorus cycle and the possibility of human-caused large-scale ocean anoxia. Phil. Trans. Math. Phys. Eng. Sci. 375 (2102), 20160318.

Wright, J.J., Konwar, K.M., Hallam, S.J., 2012. Microbial ecology of expanding oxygen minimum zones. Nat. Rev. Microbiol. 10 (6), 381–394.

Wu, C., et al., 2022. Dynamics of bacterial communities during a seasonal hypoxia at the Bohai Sea: coupling and response between abundant and rare populations. J. Environ. Sci. 111, 324–339.

Yang, Y., et al., 2021. Insignificant response of bacterioplankton community to elevated pCO_2 during a short-term microcosm experiment in a subtropical eutrophic coastal ecosystem. Front. Microbiol. 12, 730377.

Yilmaz, P., et al., 2013. The SILVA and "all-species living tree project (LTP)" taxonomic frameworks. Nucleic Acids Res. 42 (D1), D643–D648.

Zakem, E.J., Follows, M.J., 2017. A theoretical basis for a nanomolar critical oxygen concentration. Limnol. Oceanogr. 62 (2), 795–805.

Zhang, J., et al., 2010. Natural and human-induced hypoxia and consequences for coastal areas: synthesis and future development. Biogeosciences 7 (5), 1443–1467.

Zhang, W., Wu, H., Zhu, Z., 2018. Transient hypoxia extent off Changjiang River Estuary due to mobile Changjiang River plume. J. Geophys. Res.: Oceans 123 (12), 9196–9211.

Zhu, Z., et al., 2011. Hypoxia off the Changjiang (Yangtze river) estuary: oxygen depletion and organic matter decomposition. Mar. Chem. 125 (1), 108–116.

Zhu, Z., et al., 2017. Hypoxia off the Changjiang (Yangtze River) estuary and in the adjacent East China Sea: quantitative approaches to estimating the tidal impact and nutrient regeneration. Mar. Pollut. Bull. 125 (1), 103–114.

Zybailov, B., et al., 2006. Statistical analysis of membrane proteome expression changes in Saccharomyces cerevisiae. J. Proteome Res. 5 (9), 2339–2347.